

Spatial Distribution of Inputs and Local Receptive Field Properties of a Wide-Field, Looming Sensitive Neuron

Holger G. Krapp¹ and Fabrizio Gabbiani²

¹Department of Zoology, University of Cambridge, Cambridge, United Kingdom; and ²Department of Neuroscience, Baylor College of Medicine, Houston, Texas

Submitted 15 September 2004; accepted in final form 10 November 2004

Krapp, Holger G. and Fabrizio Gabbiani. Spatial distribution of inputs and local receptive field properties of a wide-field, looming sensitive neuron. *J Neurophysiol* 93: 2240–2253, 2005. First published November 17, 2004; doi:10.1152/jn.00965.2004. The lobula giant movement detector (LGMD) in the locust visual system and its target neuron, the descending contralateral movement detector (DCMD), respond to approaching objects looming on a collision course with the animal. They thus provide a good model to study the cellular and network mechanisms underlying the sensitivity to this specific class of behaviorally relevant stimuli. We determined over an entire locust eye the density distribution of optical axes describing the spatial organization of local inputs to the visual system and compared it with the sensitivity distribution of the LGMD/DCMD to local motion stimuli. The density of optical axes peaks in the equatorial region of the frontal eye. Local motion sensitivity, however, peaks in the equatorial region of the caudolateral visual field and only correlates positively with the dorso-ventral density of optical axes. On local stimulation, both the velocity tuning and the response latency of the LGMD/DCMD depend on stimulus position within the visual field. Spatial and temporal integration experiments in which several local motion stimuli were activated either simultaneously or at fixed delays reveal that the LGMD processes local motion in a strongly sublinear way. Thus the neuron's integration properties seem to depend on several factors including its dendritic morphology, the local characteristics of afferent fiber inputs, and inhibition mediated by different pathways or by voltage-gated conductances. Our study shows that the selectivity of this looming sensitive neuron to approaching objects relies on more complex biophysical mechanisms than previously thought.

INTRODUCTION

Visually guided collision avoidance is critical to the survival of many species (Gibson 1979). Accordingly, objects approaching on a collision course, or their two-dimensional projection on a screen, invariably elicit withdrawal or escape behaviors ("looming stimuli", Ball and Tronick 1971). The characteristics of neurons sensitive to looming have been studied mainly in the visual systems of insects and birds (Hatsopoulos et al. 1995; Simmons and Rind 1992; Sun and Frost 1998; Wicklein and Strausfeld 2000; reviews: Gabbiani et al. 2004; Sherk and Fowler 2001). However, little is known about the presynaptic network and biophysical properties that shape their responses (Gabbiani et al. 2002; Luksch et al. 2004).

In the locust visual system, two identified neurons, the lobula giant movement detector (LGMD) and its postsynaptic target, the descending contralateral movement detector

(DCMD), are thought to be involved in escape behavior and flight steering (O'Shea and Williams 1974; Pearson et al. 1980; Robertson and Johnson 1993; Rowell 1971). The LGMD is highly responsive to objects approaching on a collision course with the animal (Hatsopoulos et al. 1995; Judge and Rind 1997; Rind and Simmons 1992; Schlotterer 1977) but also responds to luminance changes and to small stimuli moving within its visual receptive field (Hatsopoulos et al. 1995; Rowell et al. 1977). The LGMD possesses three large dendritic fields that receive distinct inputs (O'Shea and Williams 1974). The main dendritic field integrates synaptic inputs from thousands of retinotopically arranged excitatory fibers sensitive to local motion (O'Shea and Rowell 1976). Its dendrites are arranged on a half-shell surface that intersects afferent fibers approximately perpendicularly as they enter the lobula. The remaining two dendritic fields receive local feed-forward inhibition most sensitive to large and rapid changes in luminance (Rowell et al. 1977). The LGMD membrane potential is converted into spikes, which are transferred to the DCMD in a faithful 1:1 manner via a mixed electrical/chemical synapse (Killman et al. 1999; O'Shea and Williams 1974). The DCMD, in turn, projects to the motor centers in the thoracic ganglia (Burrows and Rowell 1973). Recent studies have shown that, in the context of looming, the LGMD/DCMD firing rate peaks when a certain retinal threshold angle is exceeded (Gabbiani et al. 1999, 2001, 2002; Hatsopoulos et al. 1995; Matheson et al. 2004). Further studies support the idea that the instantaneous firing rate during looming and its characteristic peak result from a neural multiplication of excitatory and inhibitory inputs representing the instantaneous expansion velocity and size of the looming object, respectively (Gabbiani et al. 1999, 2002, 2004). Similar responses are found in nucleus rotundus neurons of pigeons (Sun and Frost 1998). Although the exact role the LGMD/DCMD plays in mediating behaviors has not yet been elucidated (Gabbiani et al. 2002; Gray et al. 2001; Hatsopoulos et al. 1995; Rind and Santer 2003), quantitative behavioral experiments in a variety of preparations indicate that angular threshold size may be the common variable used to trigger visually guided escape behaviors across many taxa (e.g., chicks, fiddler crabs: Schiff 1965; locusts: Hatsopoulos et al. 1995; Robertson and Johnson 1993; frogs: Yamamoto et al. 2003).

A detailed characterization of the properties of local inputs and their integration within looming-sensitive neurons has not yet been performed in the locust or in any other preparations.

Address for reprint requests and other correspondence: F. Gabbiani, Dept. of Neuroscience, Baylor College of Medicine, One Baylor Plaza, Houston, TX 77030 (E-mail: gabbiani@bcm.tmc.edu).

The costs of publication of this article were defrayed in part by the payment of page charges. The article must therefore be hereby marked "advertisement" in accordance with 18 U.S.C. Section 1734 solely to indicate this fact.

Earlier biophysical models have therefore approximated the LGMD as a linear summing unit directly converting inputs from its presynaptic circuitry into firing rate (Edwards 1982; Rind and Bramwell 1996). Recent indirect evidence suggests, however, that the integration of excitatory synaptic inputs within the LGMD may be nonlinear (Gabbiani et al. 2001, 2002). To investigate more directly the integration properties of the LGMD as a model for a class of looming sensitive neurons (Hatsopoulos et al. 1995; Sun and Frost 1998), we took advantage of a useful feature of insect compound eyes: it is possible to measure the orientation of optical axes in space associated with each individual ommatidium and its photoreceptors. The distribution of optical axes indicates how the retina samples visual space and can be compared with the local motion sensitivity of the LGMD/DCMD. We then characterized how the speed tuning and the interactions of local excitatory inputs affect the firing rate of the LGMD/DCMD.

METHODS

Measurements of optical axes

To determine how visual space is sampled by photoreceptors of the locust visual system, we reconstructed the distribution of optical axes associated with the mosaic of facet lenses over an entire eye (Stavenga 1979). A complete eye reconstruction was necessary because the LGMD receptive field covers most of the visual hemisphere corresponding to an entire eye (Rowell 1971). A female locust (*Schistocerca gregaria*) was fixed sidewise with bee's wax to a holder placed in the center of a goniometer. To reduce breathing movements, a ligature was made between the second and third abdominal segments. We used an eye-piece equipped with a reticule that was mounted on the goniometer to orient the animal according to anatomical markers. In a first step, we adjusted the three rotational degrees of freedom of the head. Specifically, head roll was adjusted by aligning the horizontal line of the reticule parallel to the two frontal carinae. Pitch and yaw were adjusted by aligning the vertical line of the reticule with the vertical pigment stripes and the posterior rim of the eye, respectively. In a second step, we positioned the head of the animal so that the goniometer's vertical axis, i.e., the axis through its pole, pointed at the center of the lateral eye surface. The center was defined by its projections halfway on the two line segments bounded by the eye's maximal dorso-ventral and anterior-posterior extent, respectively. The eye equator was then defined as the great circle perpendicular to the vertical pigment stripes passing through the center of the lateral eye surface.

After this centering procedure, a high-resolution digital camera (Nikon D1) was mounted on the goniometer. The orientation of the camera's optical axis was described in spherical coordinates by two angles: elevation (measured with respect to the fronto-lateral plane) and azimuth (measured around the top axis from the front; Fig. 1A). Both angles could be adjusted independently. The vertical axis of the goniometer coincided with the lateral axis (labeled in Fig. 1A) passing through the center of the eye, as explained above.

The orientation of optical axes was determined by taking two photographs at each measuring position. The first photograph was taken at the level of the deep pseudopupil (DPP), which is a virtual image that appears as an extended dark spot in the focal plane corresponding to the intersection of the optical axes at the center of the eye (Fig. 1B, top; Franceschini and Kirschfeld 1971; Stavenga 1979). The center of the DPP indicates the direction (azimuth and elevation) from which the photograph was taken. The second photograph was taken at the corneal level to obtain the local arrangement of ommatidia on the eye surface (Fig. 1B, bottom). Orthodromic illumination was used to visualize the cornea and the DPPs. The two

photographs (red, green, and blue channels, 16 bit/channel, $1,312 \times 2,000$ pixels) were transferred to a personal computer (PC) for storage and subsequent analysis. Before starting data acquisition, the eye was dusted with markers (blue chalk powder), which allowed us to identify individual ommatidia in neighboring images. We took 400 ($\times 2$) photographs along parallel circles centered on the goniometer's vertical axis. The circles were separated by 7.5° in elevation measured with respect to the top-front plane of the eye. The number of measurements taken per circle was scaled with the cosine of this elevation and ranged from 36 in the top-front plane to 5 for the circle closest to the pole of the lateral axis on the eye surface (Fig. 1A, inset). This ensured that the measurement points were equidistant on the sphere. The same goniometer and similar data acquisition protocols were used in previous studies investigating the arrangement of optical axes in the compound eyes of water striders and flies (for further technical details, see Dahmen 1991 and Petrowitz et al. 2000). The data acquisition protocol took 24 h, during which the quality of the images did not deteriorate.

Reconstruction of the arrangement of optical axes

Reconstructing the distribution of optical axes from the photographs to obtain the local density of inputs required five steps. They were carried out using custom interactive programs written for the Matlab environment (MathWorks, Natick, MA) as explained in the following paragraphs.

First, the pixels with intensity below a manually adjustable threshold were selected in a restricted area of the DPP image (Fig. 1B, top, dashed square). The threshold was adjusted to isolate those pixels belonging to the DPP and their center of mass was computed (Fig. 1B, top, cross). The position of the DPP obtained in this manner was transferred to the corneal image (Fig. 1B, bottom, cross).

Second, the position of the DPP in one corneal image was mapped to neighboring images. For this purpose, two images were observed side-by-side, and common markers were identified (typically 4; arrows in Fig. 1C, top left and top right). One image was transformed using a combination of a translation, rotation, and scaling so as to minimize the mismatch between identical markers within both images (Klette and Zamperoni 1996). The DPPs could then easily be transferred across images by counting the ommatidia between their respective locations. The outcome is shown in the Fig. 1C, bottom. The bottom left panel shows an enlargement of the dashed area of the top left panel, and the corresponding area from a neighboring image after transformation is shown on the bottom right. The white crosses indicate the location of the DPPs at the corneal level (after transformation for the bottom right panel), and white stars mark ommatidia located between the two DPPs. A total of 3,453 DPPs were mapped across images using this procedure, resulting in three or four points with known angular coordinates and delimiting a triangle or a quadrangle in each corneal image.

Third, the positions of facets within each such triangle or quadrangle were mapped to the sphere by a local interpolation procedure. For this purpose, the coordinates of the facets in the image plane were first mapped onto a plane tangent to the sphere and perpendicular to the unit vector corresponding to the DPP in the considered image. The mapping was uniquely determined as a projective (affine) transformation by the coordinates of the four (3) DPPs in each plane. The positions of the facets on the sphere were obtained by stereographic projection. A total of 314 local maps of facet directions were obtained in this way.

Fourth, the facet positions in adjacent local maps were transformed across images using the method outlined in step 2. This allowed us to check for missing facets and for inconsistencies across local map boundaries.

Fifth, the local maps were plotted in a single two-dimensional graph using a Mercator projection. This representation was used to align rows of facets across local maps. Typically, misalignments of facet

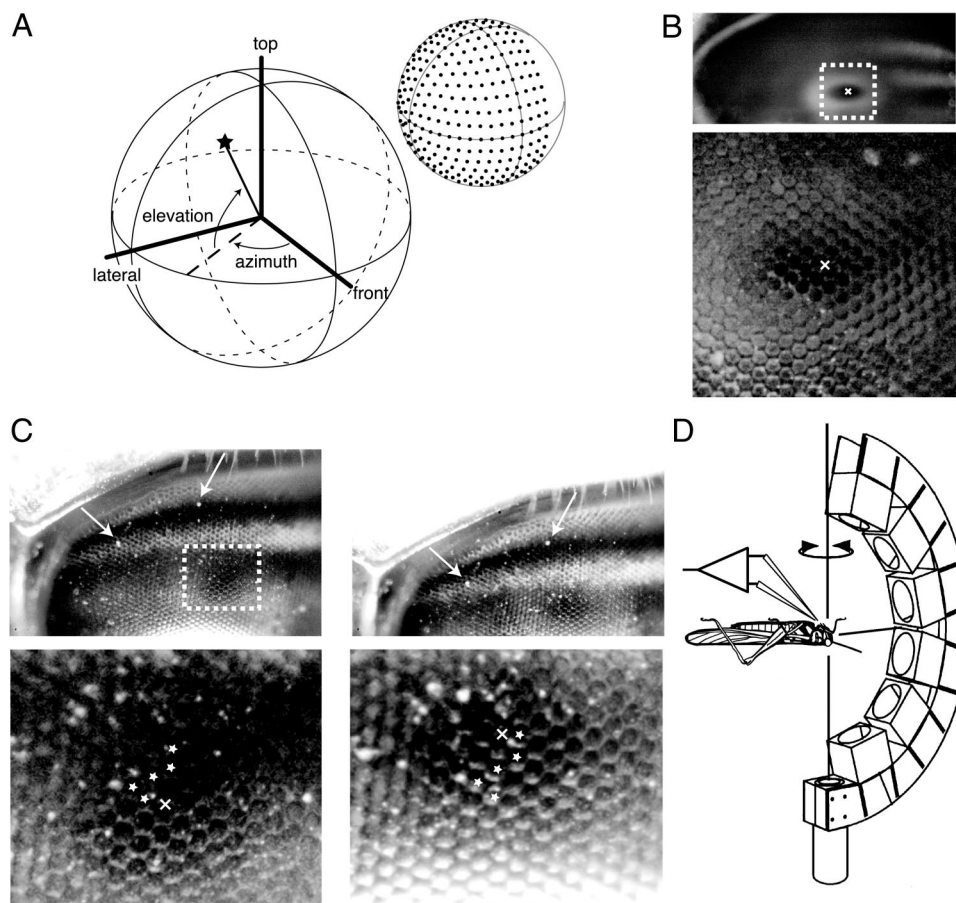


FIG. 1. Determining the density of optical axes and the sensitivity to local motion within the lobula giant movement detector (LGMD)/descending contralateral movement detector (DCMD) receptive field. *A*: coordinate system used to describe direction of optical axes in visual space. The 3 coordinate axes, labeled according to their viewing directions (top, front, and lateral), pass through the center of the eye. Elevation is measured with respect to the fronto-lateral plane and azimuth around the top axis. The angular position with azimuth and elevation equal to 0° corresponds to the direction pointing directly in front of the animal. Negative and positive elevations describe ventral and dorsal parts of the visual field with respect to the eye equator, respectively. *Inset*: each dot represents an angular position from which photographs of the cornea and deep pseudopupil (DPP) were taken. *B*: coordinates of DPPs (white cross in framed region, *top*) were determined from the center of mass of its dark core. These coordinates were mapped onto the corneal level (white cross, *bottom*). *C*: to map the DPPs from 1 image to an adjacent one, we identified common markers in both images (white arrows, *top left* and *right*). Images were put in register using a transformation computed from the marker positions. *Bottom left*: magnification of the area delimited by dashed white box in the *top left* image. *Bottom right*: corresponding area in the 2nd image after registration. Crosses in both images indicate DPPs in neighboring images. Stars indicate matching facets between the 2 DPPs. *D*: stimulation during electrophysiological recordings was achieved by placing the locust upside down at the center of an apparatus equipped with 6 local stimulators mounted at different elevations. Azimuth of the stimulators was changed by rotation of apparatus around the vertical axis (adapted from Krapp and Hengstenberg 1997).

rows across different maps were less than one facet and could easily be corrected. These misalignments were mainly caused by the variability in selecting pixel positions of DPPs with mouse-clicks by the operator. In three cases, larger mismatches were found (on the order of 2–3 facets), suggesting genuine errors in DPP mapping. Those errors were due to the lack of clear markers between images but did not compromise the general findings (see DISCUSSION).

Practical implementation

The transformations described in steps 2 and 3 were implemented using the image registration routines of the Image Processing toolbox (Mathworks). Similarly, various contrast enhancement techniques were applied to the green or red channel of the images to facilitate the identification of single facets and markers.

We confined ourselves to analyze a single eye. Earlier partial reconstructions of invertebrate compound eyes have shown consistent results across animals (water strider: Dahmen 1991; locust: Horridge 1978; fly: Beersma et al. 1975, 1977; Land and Eckert 1985; Petrowitz et al. 2000). To assess the variability of our measurements, we first

repeated the entire alignment procedure of a single female animal in the goniometer five times and determined after each alignment the corneal position of the DPP at four locations (90° az., 0° el.; 90° az., 90° el.; 135° az., 0° el.; 90° az., -45° el.). On average, the variability in the corneal position of these DPPs was less than one facet. We next performed the same four measurements on five different female animals and inspected the local arrangements of facet rows at the corneal positions of the DPPs. The orientation of facet rows was consistent across animals and the variability was similar to that described in the fly by Petrowitz et al. (2000).

Density map

The density of optical axes was computed on a $2 \times 2^\circ$ grid over the entire eye. The number of optical axes in a 10° spherical cap centered at each point of the grid was determined and divided by the cap area to obtain the density per unit solid angle. The solid angle area was expressed in squared degrees and the density is reported in units of (optical axes/deg²). The size of the cap was chosen to match the

spherical area stimulated locally during electrophysiological experiments (see *Visual stimulation* below).

Dissection and electrophysiology

We recorded the spiking activity of the DCMD at the level of the cervical connective using extracellular hook electrodes. The animals were fixed upside down to a holder with tape and bee's wax, which allowed us to orient the head according to reliable anatomical markers as described above. We opened the ventral neck, removed air sacks, and cleaned the connective contralateral to the stimulated eye. Once a stable recording was established, we covered the electrodes and the neck wound with petroleum jelly to insulate the electrodes and prevent the preparation from drying out. Recordings were performed using standard electrophysiological equipment. DCMD spikes were easily thresholded because of their large amplitude and were converted into unit pulses sampled at a frequency of 0.72 kHz by an A/D board (DT2801, Data Translation) and transferred to a PC. Data acquisition and visual stimulation (see *Visual stimulation*) were controlled using dedicated software (ASYST, Macmillan). The longest stimulus protocols took 4–5 h, within which the recordings remained stable.

Visual stimulation

Many earlier studies focused on the looming sensitivity of the LGMD/DCMD by presenting approaching objects on a collision course with the animal. For these stimuli, both the angular size and the expansion velocity simultaneously change over time. In contrast, we chose a local motion stimulus whose angular size was constant but whose velocity was systematically varied as specified below. Using such local motion stimuli allowed us 1) to keep the neuron's response well below its saturation level, a necessary prerequisite when mapping the neuron's sensitivity profile throughout its receptive field; 2) to study the speed dependence of the neuron's response to local motion; 3) to focus on the spatial and temporal integration of local excitatory inputs; and 4) to test whether the LGMD/DCMD responds to local motion in a directionally selective way.

During electrophysiological experiments, we placed the locust in the center of a vertical semicircular apparatus. Six independent stimulators were mounted on the meridian frame at elevations ranging from -75° to $+75^\circ$ and a spacing of 30° . The frame could be moved around the animal to stimulate different azimuths (Fig. 1D). The azimuths employed ranged from 0 (frontal stimulation) to 180° (caudal stimulation) in steps of 30° (e.g., Fig. 3A). Each stimulator was equipped with a step motor that moved a black disc (7.6° diam) in front of a white background (contrast > 80%) along a circular path (10.4° diam). Further details can be found in Krapp and Hengstenberg (1997). The speed of disc motion, v , was set to 0.2, 0.5, 1.0, 2.0, or 4.0 cycles per second (c/s) depending on the stimulus protocol. Consecutive stimuli applied at the same azimuth but different elevations were separated by an interstimulus interval of 5 s. An interval of ≥ 30 s separated stimuli applied at different azimuths, as the apparatus was adjusted manually to the new position. In all the protocols described below, stimuli applied at the same spatial location were always separated by an interstimulus interval of ≥ 60 s. We performed preliminary experiments on two animals to verify that this stimulus interval was sufficient to minimize local habituation (O'Shea and Rowell 1975), irrespective of stimulus position.

Stimulation protocols

The first protocol was designed to assess the spatial sensitivity of the LGMD/DCMD to local motion stimuli. The moving disc was presented at 36 different stimulus positions (Fig. 3A). During this protocol, each position was stimulated four times at five different speeds (0.2, 0.5, 1.0, 2.0, and 4.0 c/s). For a given speed and position,

we moved the stimulus two times in both counterclockwise and clockwise directions (Fig. 3B, *left insets, 1–4*). A total of six female animals were used.

The second protocol was designed to study the summation of response to two local motion stimuli presented simultaneously in the LGMD/DCMD receptive field. We first measured the response to individual disc motion at all six elevations and an azimuth of 90° . Subsequently, two discs were activated simultaneously. One of the two discs was always presented at the same location, either at an elevation of -45° or -15° . The position of the second disc was systematically varied over the remaining five elevations. The speed of disc motion was equal to 2.0 c/s and each measurement was repeated five times on five animals (1 male and 4 females). An additional five female animals were tested at a disc speed of 0.2 c/s.

The third protocol investigated the summation of response to an increasing number of simultaneously presented local motion stimuli. As in the previous protocol, we first measured the responses to individual disc motion at all six elevations and an azimuth of 90° . Next two, four, and six discs were moved simultaneously using two different spatial arrangements. In the first one, the number of stimuli increased from the dorsal and ventral periphery toward the center of the visual field. The activated stations had elevations of $(-75^\circ, +75^\circ)$, $(-75^\circ, -45^\circ, +45^\circ, +75^\circ)$, and $(-75^\circ, -45^\circ, -15^\circ, +15^\circ, +45^\circ, +75^\circ)$, respectively (Fig. 1D). In the second arrangement, the number of stimuli increased from the center toward the periphery and the elevation of activated stations were $(-15^\circ, +15^\circ)$, $(-45^\circ, -15^\circ, +15^\circ, +45^\circ)$, and $(-75^\circ, -45^\circ, -15^\circ, +15^\circ, +45^\circ, +75^\circ)$. Each measurement was repeated five times on five animals (1 male and 4 females) at a disc speed of 2 c/s. An additional five female animals were tested at a disc speed of 0.2 c/s.

The fourth protocol studied the impact of the time difference between the activation of two consecutive local motion stimuli presented at neighboring positions. A disc moving at 0.5 c/s at an elevation of -15° was followed after 1, 50, or 100 ms by the activation of a second disc moving at 2.0 c/s at an elevation of -45° . The responses to both discs stimulated individually were also measured. Each of these measurements was repeated five times on five different animals (1 male and 4 females). The delay of 1 ms was approximately equivalent to simultaneous activation as used in the previous two protocols and allowed us to test for a potential influence of local speed on spatial summation. The other two delay and speed values were selected because they were in the range corresponding to the retinal speed increase typically experienced by the edge of an object such as a square approaching at a constant speed along the lateral axis at the two stimulated positions (Gabbiani et al. 1999). This may be seen by converting the rotational disc speed to an equivalent retinal speed by taking into account the length of the circular path in visual space (32.6° ; obtained by multiplying the path diameter, 10.4° , by π). Using this conversion formula, the two retinal speed values corresponding to 0.5 and 2.0 c/s amount to 16.3 and 65.2 deg/s, respectively. Such retinal speeds are reached 416 and 203 ms prior to collision for an approaching square if the square half edge length divided by its approach speed equals 50 ms. At these two time-points, 416 and 203 ms prior to collision, the corresponding object angular size amounts to 13.8° and 27.6° , respectively. During the interval separating them (~ 200 ms, as well as during shorter ones when the ratio of the square's half edge length to approach speed is smaller), there is significant summation of excitation in the LGMD during looming (e.g., Fig. 2 of Gabbiani et al. 1999).

Analysis of electrophysiological data

To determine the sensitivity of the LGMD/DCMD neurons' response to the visual stimulus, we analyzed the data within a 250-ms time window starting at stimulus onset. Because the maximal speed of disc motion was 4 c/s, the stimulus passed at most once over each location on the eye. The length of the window was selected to

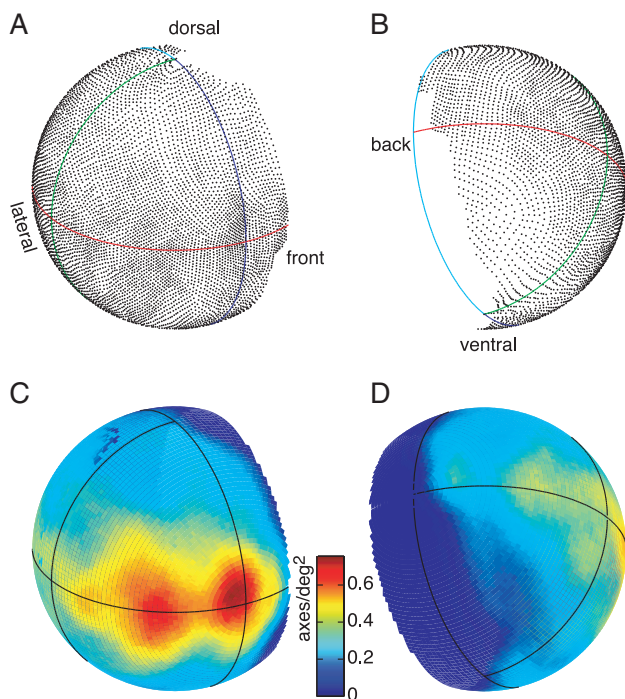


FIG. 2. Spherical representation of the direction and density of optical axes from an entire locust eye. Each dot in *A* and *B* indicates the intersection of an individual optical axis with the surface of the sphere, as seen from a dorso-lateral and ventrocaudal perspective, respectively. Red line indicates the eye equator; blue and green lines indicate the 0 and 90° azimuth great circles. *C* and *D*: color-coded density of optical axes (axes/deg²). Red indicates areas of highest and dark blue areas of lowest density. Maximal frontal density was 0.76 axes/deg². Lateral density was 0.39 axes/deg² (see Fig. 1*A* for axes labels). Density at the midpoint between lateral and front axes on the eye equator was 0.63 axes/deg². It was 0.28 axes/deg² at the midpoint on the 90° azimuth great circle between the lateral and top axes.

minimize habituation effects (see RESULTS). We first determined the mean firing rate over the 250-ms interval. Next, we estimated the instantaneous firing rate by convolving the spike train with a Gaussian ($\sigma = 20$ ms) and normalizing by the number of spikes over the interval. Finally, we computed the instantaneous firing rate as the inverse of the interspike intervals (ISIs). Several authors have discussed the significance of these measures (e.g., Pauluis and Baker 2000; Richmond et al. 1990). The total number of ommatidia stimulated during a 250-ms time window depends on the speed of disc motion. To assess whether this might have an effect on the results, we also computed the mean and instantaneous firing rate estimates over variable time windows corresponding to one-quarter, one-half, three-quarters, or a full cycle of disc motion. All subsequent data analyses were then repeated using these alternate values.

The sensitivity plots shown in Fig. 4, *A* and *B*, were obtained by interpolating the mean and ISI-derived peak firing rates from the experimental data grid (30 × 30° spacing) to a 15 × 15° grid using cubic splines. In Fig. 6, the mean firing rate data points (average across 6 animals at 1 c/s) were interpolated using the same technique.

To characterize the dependence of mean firing rate on stimulus speed, we computed mean responses across trials and experiments and fitted this data at each stimulus location as a function of the base 2 logarithm of normalized stimulus speed, $\log_2(v/v_{\max})$, $v_{\max} = 4$ c/s. The base 2 logarithm was chosen because it facilitated interpretation, given the specific values of stimulus speed chosen [$\log_2(v/v_{\max}) = -4.32, -3, -2, -1, \text{ and } 0$ when $v = 0.2, 0.5, 1, 2, \text{ and } 4$ c/s, respectively]. The fit was performed independently at each spatial stimulus location by least squares. The goodness of fit was assessed by

computing χ^2 values using SDs computed across experiments (Press et al. 1992).

To characterize the latency of DCMD responses, we computed for each animal the median latency as a function of azimuth and speed. The median was computed across all trials obtained at the four elevations available for each azimuth (± 15 and $\pm 45^\circ$). Medians were used because of their robustness to outliers. The median values obtained in this way were averaged across six animals.

The results of spatial summation experiments presented in Fig. 8 were analyzed over a fixed time window of 500 ms. Similar results were obtained over a 250-ms time window. In all experiments, the results were independent of the sex of individual animals, as expected from observations made in earlier studies (Gabbiani et al. 1999). Data were thus pooled across sexes.

Finally, the data sets obtained using the first protocol were analyzed by applying the method proposed by Krapp and Hengstenberg (1997) to determine the local preferred directions and motion sensitivities in fly visual interneurons.

The Pearson correlation coefficient is abbreviated by ρ throughout. All programs for data analysis were written using Matlab.

RESULTS

Density of optical axes in the locust compound eye

The density of optical axes was determined over the entire compound eye of one female locust (*Schistocerca gregaria*). Figure 2, *A* and *B*, shows the orientation of optical axes from an upper frontolateral and lower caudolateral perspective, respectively. Each dot indicates the point of intersection between an individual optical axis and the surface of a sphere representing visual space. In total, we determined the orientation of 7,317 individual optical axes across 314 different patches on the eye surface [23.3 ± 10.8 (SD) facets/patch, minimum: 4, maximum: 75]. The density distribution of optical axes sampling the visual field varies markedly across the eye (Fig. 2, *C* and *D*). We found an acute zone in this unisotropic sensitivity distribution with a maximum density of 0.76 axes/deg² in the fronto-equatorial region. Along the eye equator, there is a streak of high density that gradually decreases toward the caudal rim of the eye. The density also decreases from the eye equator toward the dorsal and ventral parts of the eye. The fronto-equatorial visual field has an area of binocular overlap of about 15–20° (Fig. 2*C*). The animal's head restricts the visual field in a caudal area below the eye equator, due to the eye position on the head (Fig. 2*D*).

Characterization of the DCMD responses to local motion stimuli

Figure 3*A* shows a typical example in one animal of the DCMD spiking activity in response to the motion stimulus depicted in Fig. 1*D*. The stimulus was presented at 36 different positions within the DCMD receptive field, and each rectangular box in Fig. 3*A* corresponds to one such position (disc speed: 2 c/s). At stimulus onset, the DCMD generated a response that decreased in a position-dependent manner (Fig. 3*A*). Several consecutive cycles of dot motion resulted in complete habituation of the response, confirming well-known habituation properties (e.g., O'Shea and Rowell 1975). The four rasters in response to stimulation at +150° azimuth and +15° elevation (shaded box in Fig. 3*A*) are plotted above the time axis in Fig. 3*B*. The direction of disc motion for each trial is shown on the left (*insets*). Taking into account the direction

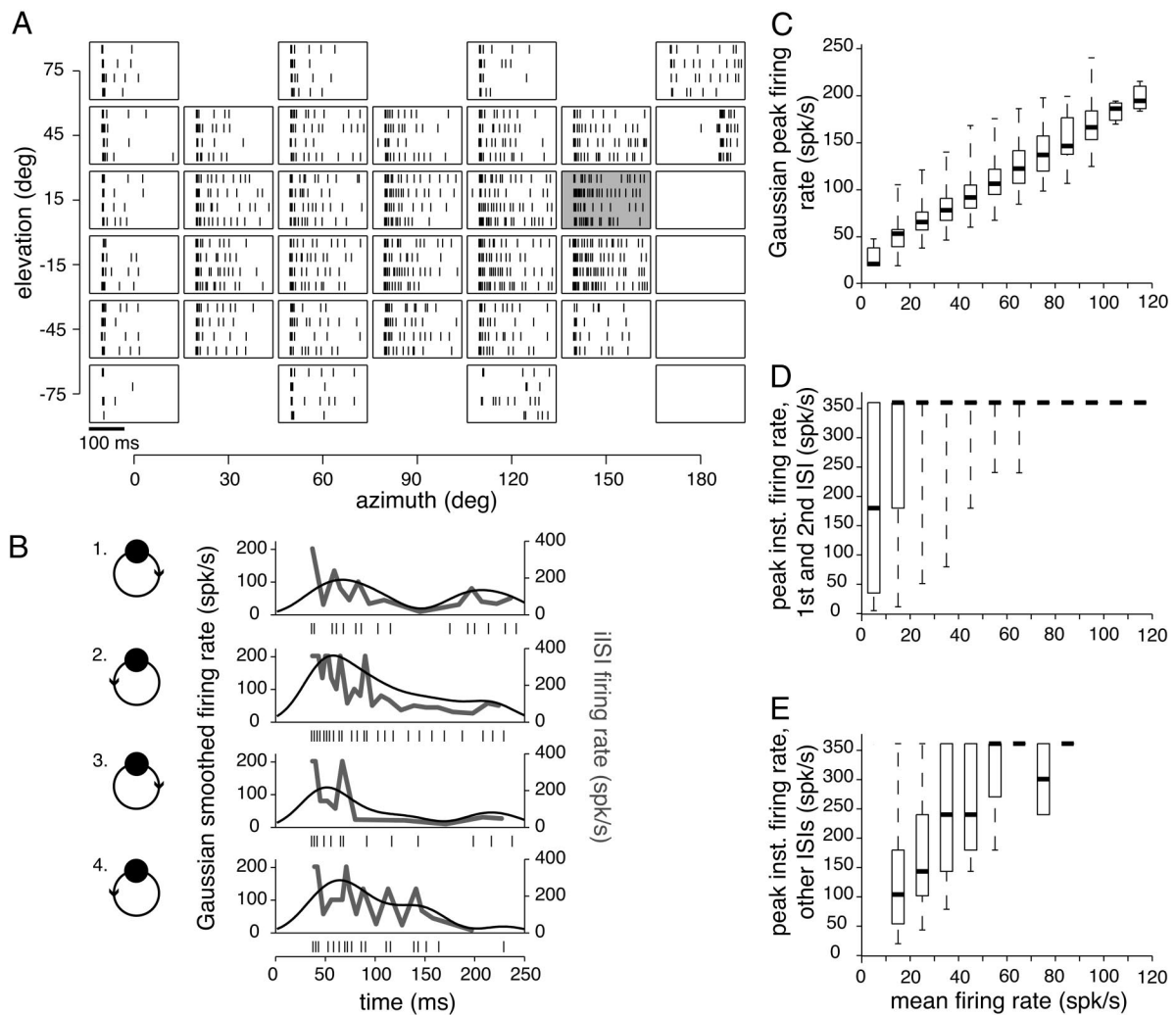


FIG. 3. Responses to a black disc moving at 2 c/s. *A*: raster plots. Each box corresponds to a different position (azimuth, elevation) over the animal's right eye. Each line is a different trial and each vertical bar indicates a spike recorded within the 1st 250 ms after stimulus onset. *B*: responses obtained at 150° azimuth and 15° elevation (gray box in *A*). Dot stimulus was moved alternatively in clockwise (trials 1 and 3) and counterclockwise direction (trials 2 and 4; insets to left). Corresponding 4 spike rasters are shown at the bottom of each panel. Estimates of the instantaneous firing rate obtained by Gaussian smoothing (left ordinate) and from individual interspike intervals (ISIs; right ordinate) are shown on top for each trial (black and gray curves, respectively). Note the different scaling of the respective ordinates. *C*: distribution of Gaussian smoothed peak firing rate as a function of mean firing rate (10 spikes/s bins). Thick horizontal bars indicate medians, boxes delimit the upper and lower quartiles, and dashed vertical bars give the range of experimental values. *D*: estimate of peak instantaneous firing rate computed from the 1st and 2nd ISIs as a function of the mean firing rate (same plotting conventions as in *C*). *E*: peak instantaneous firing rate obtained from the ISIs (excluding the 1st and 2nd ISIs) as a function of mean firing rate. (*C*–*E* include data pooled from 6 different animals at 5 speeds.)

of disc motion did not reveal any significant local directional preferences of the DCMD over its receptive field (Fig. 3*A*). This contrasts with results in many fly lobula plate interneurons (e.g., Krapp et al. 1998), but is consistent with the lack of directional selectivity reported in the DCMD for extended stimuli, such as bars sweeping in different directions over the eye.

To characterize the temporal dynamics of the response, we computed estimates of the instantaneous firing rate using two different methods: Gaussian smoothing (Gs) and calculation of the iISI. Both estimates are plotted as a function of time above each raster in Fig. 3*B* (gray curve and right ordinate for iISI firing rate; black curve and left ordinate for Gs firing rate). The overall shape of these curves was similar but revealed some important differences. The iISI firing rate was very irregular and reached peak activities of similar or identical amplitude at several points in time. On average, the iISI firing rate differed

by a factor of almost two from the Gs firing rate (compare the left and right ordinates in Fig. 3*B*). Figure 3*C* shows the distribution of Gs peak firing rates as a function of mean firing rate for single trials, pooled across six animals at five speeds. The relationship between these two variables was very close to linear ($\rho = 0.99$). Such a linear relationship could not be found when the distribution of the peak iISI firing rate was plotted against mean firing rate. This was mostly due to the fact that the DCMD fired a few spikes in rapid succession locked to the onset of stimulation (Fig. 3*A*). The first and second ISIs of this transient "onset" response were typically very short and determined the peak iISI firing rate in many trials (e.g., Fig. 3*B*). Figure 3*D* shows this point by plotting the distribution of the iISI firing rate as a function of mean firing rate when only the first and second ISIs of a response are taken into account. Except for outliers (dashed lines), the distribution saturates at 360 spikes/s when the mean firing rate exceeds 30 spikes/s.

Accordingly, the peak of the iISI firing rate computed without considering the first and second ISIs was much better correlated with the mean firing rate ($\rho = 0.89$, Fig. 3E). Thus the response of the DCMD to disc motion typically consisted of a high-frequency transient onset response of two to three spikes followed by a sustained, irregular response that could be characterized equally well by the peak Gaussian firing rate or the mean firing rate and which did not depend on the exact length of the time window analyzed. When the first and second ISIs were excluded, the peak iISI firing rate also led qualitatively to similar results in our subsequent analysis.

Spatial sensitivity and speed tuning of the DCMD's receptive field

We computed the sensitivity to local motion stimuli throughout the DCMD receptive field in six animals. Figure 4, A and B, shows characteristic examples of the sensitivity distribution obtained at a speed of 1 c/s in one animal. The mean firing rate and the iISI peak firing rate (1st and 2nd ISI excluded) are plotted over azimuth and elevation, respectively. The DCMD is sensitive to visual motion over an extended area that covers almost an entire visual hemisphere. However, the sensitivity also shows a marked unisotropic distribution for both response variables. The only slight qualitative difference between the mean firing and iISI peak firing distributions is that in the latter case the distribution is rather flat in the frontolateral area of the receptive field. As outlined in the previous section, this is due to the fact that the iISI peak firing is often determined by a singular event, i.e., one short ISI, which does not indicate subtle activity changes. We consistently found maximum sen-

sitivity in the equatorial region of the caudal receptive field (azimuth = 150°). From here, the sensitivity steeply decreases toward an azimuth of 180°, reflecting the margins of the animal's visual field. The sensitivity also decreases gradually along the equator toward the front. It becomes minimal at 0° azimuth, reflecting the frontal margins of the visual field (Fig. 4C). A second gradient is found along the elevation. From the equatorial region, the sensitivity decreases toward the dorsal and ventral parts of the receptive field, with a slightly steeper slope in the ventral direction (Fig. 4D). This basic shape of the sensitivity distribution changed only slightly with stimulus speed, although higher speeds resulted in stronger DCMD responses (Fig. 4, C and D).

Figure 5A shows the average spatial speed tuning ($n = 6$ animals). At each location, the stimulus speed, v , ranged from $v_{\min} = 0.2$ to $v_{\max} = 4.0$ c/s. The mean firing rate, f_{mean} , was well fitted at each location by a logarithmic function of speed

$$f_{\text{mean}} = \alpha + \beta \log_2(v/v_{\max}) \quad (1)$$

(mean χ^2 over spatial location: 0.62; maximum: 2.37). α represents the mean firing rate at the maximum speed for a given location, and β is the decrement for each halving of stimulus speed. Figure 5B plots the values of β as a function of α pooled over the spatial extent of the receptive field. The two parameters were highly correlated ($\rho = 0.97$) and to a good approximation, $\beta = 0.13\alpha + 0.28$. We infer from Fig. 5B that, in >80% of the fits, $\alpha > 10$ spikes/s and therefore the second term in $\beta = 0.13\alpha + 0.28$ is typically small compared with the first one (<20%). Inserting this relation in Eq. 1 and neglecting

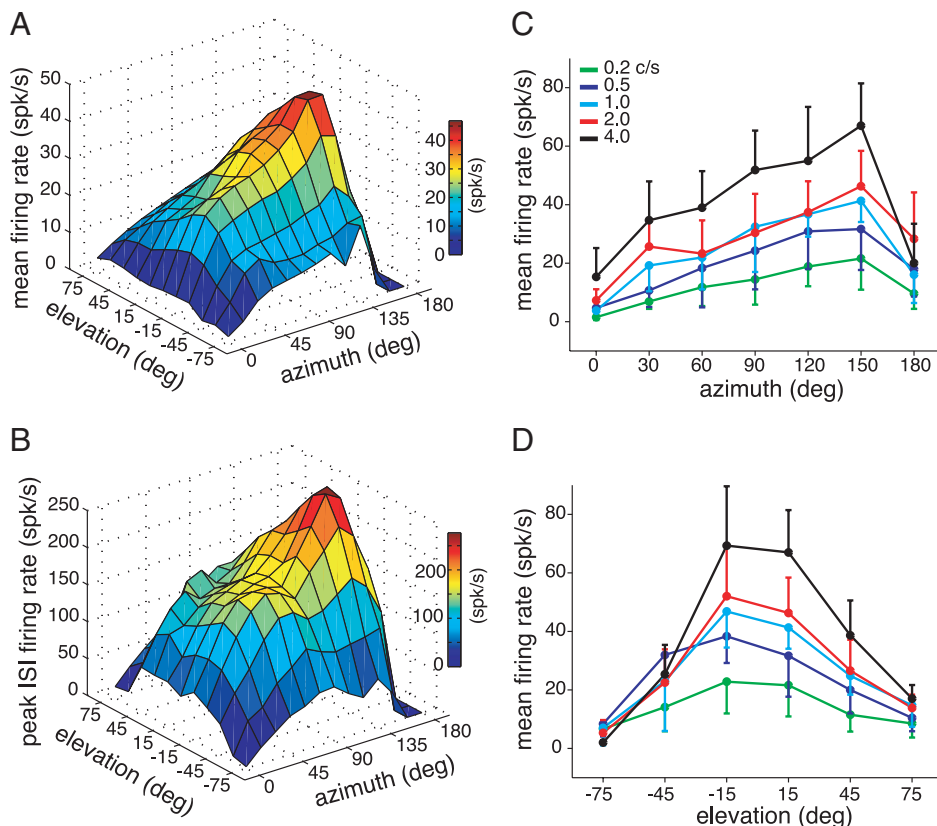


FIG. 4. Spatial sensitivity distribution to local disc motion. A and B: mean firing rate and iISI peak firing rate obtained from 1 animal as a function of stimulus position (disc speed: 1 c/s). C and D: sections through average distribution across 6 animals along azimuth (C, 15° elevation) and elevation (D, 150° azimuth). Individual data points give mean values, and error bars indicate SD. Different colors denote different stimulus speeds from 0.2 to 4.0 c/s.

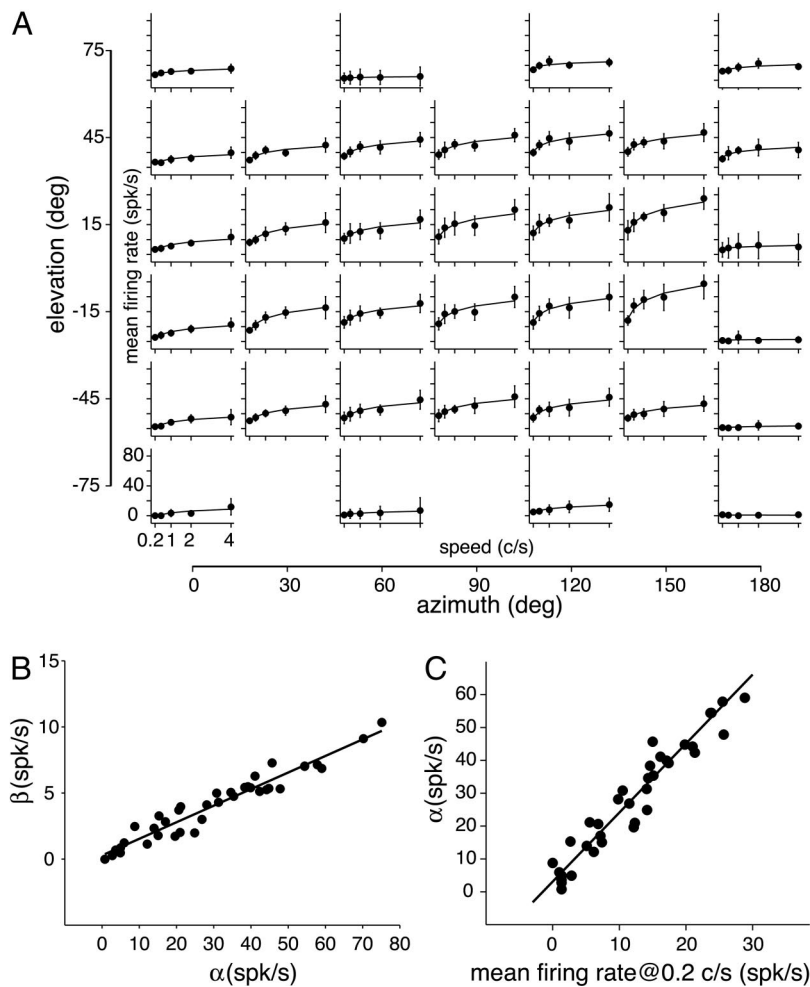


FIG. 5. Characterization of local speed tuning. *A*: mean firing rate as a function of disc speed. Each subpanel corresponds to a different azimuth and elevation. Black dots report the mean firing rate (average over 6 animals), and error bars show SD. Solid lines are fits with the function $f_{\text{mean}} = \alpha + \beta \log_2(v/v_{\text{max}})$. *B*: plot of the fit parameter β as a function of α . Black line is the linear fit between these 2 variables ($\beta = 0.13\alpha + 0.28$, $\rho = 0.97$). *C*: plot of the fit parameter α as a function of mean firing rate at 0.2 c/s. Black line is the linear fit between these 2 variables ($\rho = 0.97$). If we denote by γ the mean firing rate at 0.2 c/s, it is given by $\alpha = 2.10\gamma + 3.06$.

the constant term yields a simple approximation valid over most of the receptive field

$$f_{\text{mean}} = \alpha[1 + 0.13 \log_2(v/v_{\text{max}})] \quad (2)$$

at the expense of a slightly decreased fit performance (mean χ^2 over spatial location: 1.46; maximum: 9.54). This last equation states that the mean firing rate is reduced by about 13% of its peak value for each halving of stimulus speed. At the lowest velocity of 0.2 c/s, the factor in squared brackets in Eq. 2 equals 0.44, and speed sensitivity is divided on average by slightly more than a factor two over the entire receptive field. Figure 5C plots the mean firing rate at 4 c/s (i.e., the parameter α) as a function of the mean firing rate at 0.2 c/s over the spatial extent of the receptive field. These two variables were linearly related ($\rho = 0.97$) with a slope of 2.1, corresponding to an average reduction in sensitivity of 0.48, in good agreement with Eq. 2.

Analyzing the data in terms of peak firing rates (Gs and iISI) or over a time window corresponding to a fraction of the stimulus cycle (see METHODS) led to qualitatively similar results, with a few quantitative differences. For example, when a time window corresponding to a full rotation cycle was selected, the mean firing rate at 0.2 c/s varied over a smaller range (0–5 spikes/s) than that obtained over a 250-ms window. In contrast, the mean firing rate at 4 c/s reached similar peak values. This led to a linear relationship ($\rho = 0.94$) between the

mean firing rate at 4 c/s and that at 0.2 c/s similar to that reported in Fig. 5C, but with a steeper slope. If we denote by γ the mean firing rate at 0.2 c/s over the full rotation cycle, the optimal linear fit was given by $\alpha = 10.0\gamma + 5.6$. Correspondingly, the linear relation between α and β was maintained over the full rotation cycle ($\rho = 0.99$) but with a stronger decrement for each halving of stimulus speed ($\beta = 0.23\alpha + 0.20$).

Correlation between optical axes density and spatial speed tuning

For a disc moving at a fixed speed, the density of optical axes serves as an indicator for the number of local inputs activated in the excitatory dendritic field, since the LGMD receives inputs from the entire array of retinotopic visual afferents originating in the medulla. A straightforward prediction would therefore be that the sensitivity of the DCMD to motion stimuli should be correlated with the density of local inputs. This prediction relies on the assumption that the number of locally activated inputs plays a dominant role in determining the response of the LGMD/DCMD as opposed to other biophysical factors. This seems reasonable given the tight correlation often observed between dendritic anatomy, afferent density, and receptive field structure as reported for example in some fly lobula plate tangential neurons (Krapp et al. 1998) and in interneurons of the cricket cercal system (Jacobs and Theunissen 2000).

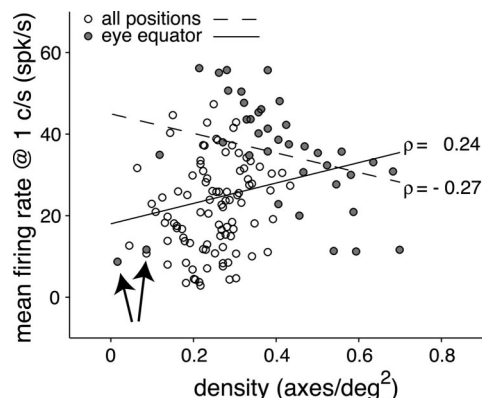


FIG. 6. Correlation between optical axes density and local motion sensitivity. Mean interpolated firing rate in response to disc motion (1 c/s) is plotted as a function of optical axes density. Gray circles denote densities along the eye equator; open circles denote all positions. Regression lines were fitted to data along the eye equator (dashed line) and to all data (straight line). Sensitivity was averaged for each position across 6 animals. Arrows denote 2 measurements close to the eye equator (elevations of 0 and 15°) in the back of the eye (azimuth of 180°).

To address this question, we compared directly the visual axes density to motion sensitivity of the DCMD. Figure 6 plots the sensitivity to disc motion across the DCMD receptive field (mean firing rate over 6 animals, disc speed of 1 c/s) as a function of the corresponding density of optical axes. There is only a weak positive correlation ($\rho = 0.24$) between mean firing rate and density. This positive correlation results from a parallel drop in density and motion sensitivity from the equator toward more dorsal and ventral elevations. However, this trend is counteracted by an opposite trend along azimuth at the equator where there was a weak negative correlation between density and motion sensitivity ($\rho = -0.27$; Fig. 6, gray dots). The negative correlation was considerably stronger ($\rho = -0.69$) when two “outlier” measurements corresponding to the steep drop in motion sensitivity straight to the back of the animal were excluded (180° azimuth; arrows in Fig. 6). This result is particularly striking: mean firing rates decreased by a factor of ~ 3 in parallel with an increase in density by about the same factor along the eye equator (Fig. 6, gray circles). This reflects the fact that the motion sensitivity of the DCMD peaks in the caudal visual field (Fig. 4A), whereas the highest density of optical axes is located in the frontal visual field (Fig. 2C). Similar results were obtained for the other speeds of disc motion.

Latency of response to local motion

The pronounced spatial variations in speed sensitivity suggest that other variables, such as the latency of DCMD responses, might also depend on stimulus position. Because the DCMD typically fired a few spikes locked to the onset of disc motion, we addressed this question by computing the latency between stimulus onset and the time of first spike occurrence. The analysis was confined to data obtained from the equatorial region of the eye along the azimuth since the number of measuring positions was almost twice as extensive as along the elevation. Figure 7 plots the average median delay as a function of the stimulus azimuth at five speeds of disc motion. The latency to the first spike depended both on disc speed and on azimuth. Delays decreased with increasing speed of motion

and reached a minimum at 2 c/s followed by a slight increase at 4 c/s. Interestingly, the response delay also decreased with increasing azimuth. Stimulation in the frontal visual field (azimuth = 0°) resulted in the longest response delays at all stimulus speeds. The delay decreased as stimulation took place at more posterior positions and saturated at azimuth values $\geq 60^\circ$.

Spatial summation of local motion stimuli

We investigated the spatial summation of local motion stimuli by displaying them simultaneously in several positions of visual space. The mean firing rate was first measured as a function of elevation at an azimuth of 90° for a single disc rotating at a speed of 2 c/s (Fig. 8A). We then activated two stations simultaneously: one was located at an elevation of -15° , whereas the position of the second one was varied among the remaining five locations. The mean firing rate measured under these conditions is plotted in Fig. 8B as a function of the linear prediction obtained by summing the single station responses reported in Fig. 8A (black circles). Each data point lies clearly below the diagonal (dash-dotted line), indicating a strongly sublinear summation. Strikingly, the measured mean firing rate was only slightly higher than the response elicited by a single stimulation at -15° elevation (Fig. 8A, black circle at -15° elevation) and independent of the particular position of the second stimulus (Fig. 8B, filled circles in insets). The same result was obtained when the position of the first station was changed to -45° (Fig. 8C). Responses were again only slightly higher than those elicited by a single stimulation at -45° elevation (Fig. 8A, black circle at -45° elevation) and independent of the particular position of the second stimulus. To verify that this strongly sublinear summation was not due to a saturation of responses, we repeated these experiments at a speed of 0.2 c/s and obtained identical results to those depicted in Fig. 8, B and C (data not shown).

We next investigated in five animals whether activation of more than two simultaneous stations might alter the summation scheme. Figure 8, D and E, shows the outcome of two experiments in which either two, four, or six stations were stimulated simultaneously, whereas Fig. 8A reports the mean responses to

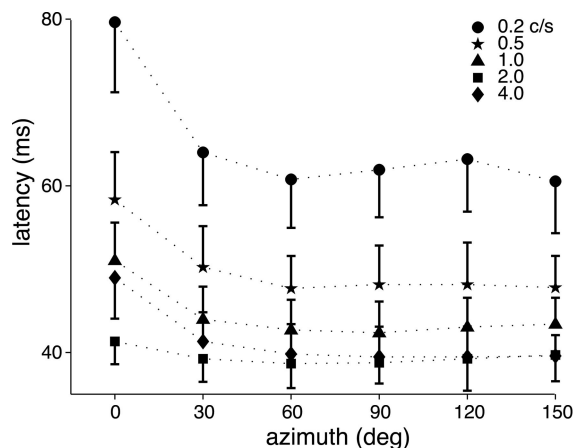


FIG. 7. Latency between stimulus onset and the 1st spike recorded in the DCMD. Median latencies (from 6 different animals) are plotted against azimuth (error bars = \pm SD). Different symbols indicate different stimulus speeds.

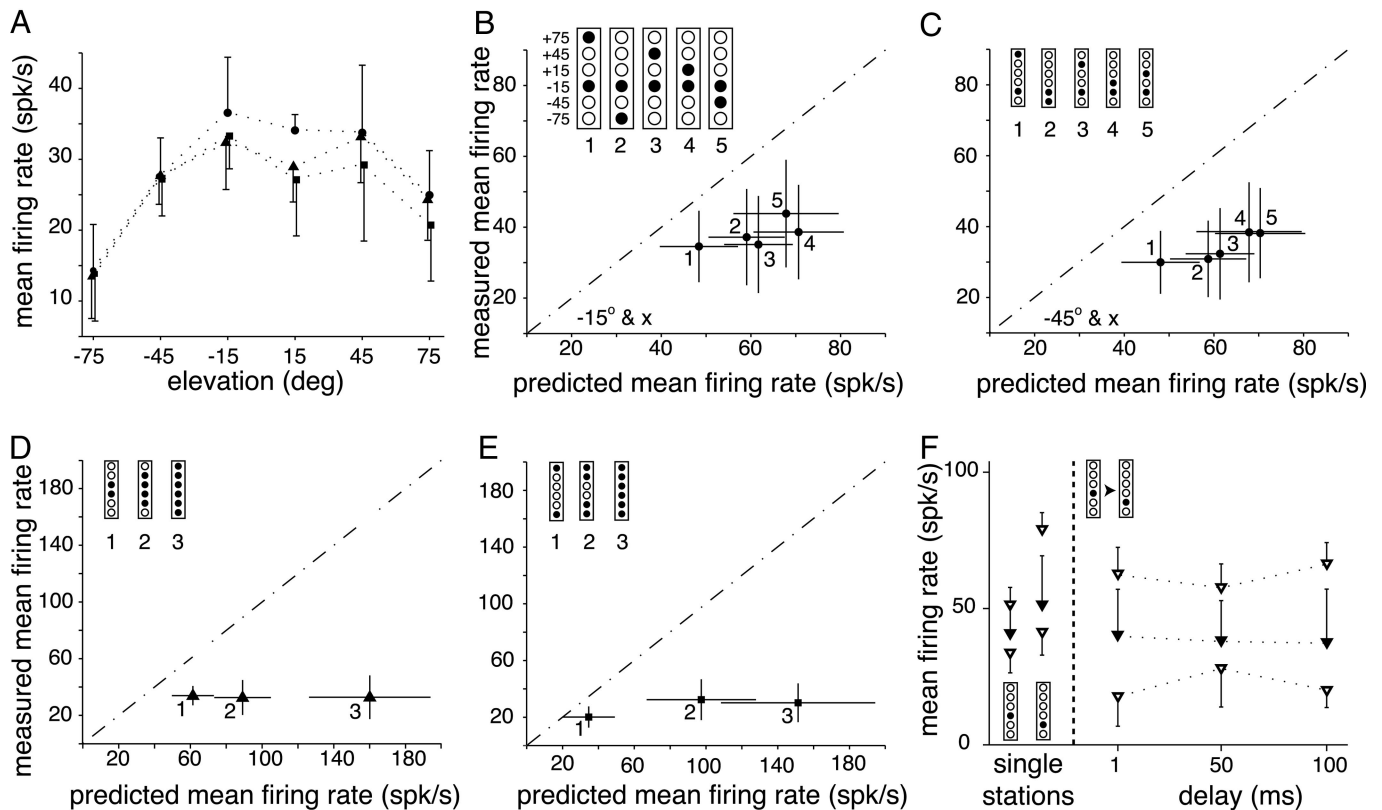


FIG. 8. Spatial and temporal integration of responses to local disc motion. *A*: mean response (\pm SD) across 5 animals to individual disc motion as a function of elevation (90° azimuth). The 3 different curves and associated symbols correspond to responses acquired separately for each of 3 experiments reported in *B* and *C* (\bullet), *D* (\blacktriangle), and *E* (\blacksquare). *B*: responses to 2 simultaneously presented stimuli as a function of the linear prediction from responses to individual disc motion (obtained from *A*). One of the stimuli had a fixed elevation (-15°), whereas the 2nd stimulus was presented at each of the other 5 positions (points labeled 1–5). In this and following plots, schematic drawings corresponding to each point (top left) indicate the elevation of the stimuli by black dots. *C*: experiment with the same design as *B*, except that the fixed stimulus was at -45° . *D*: responses to an increasing number of disc stimuli plotted as a function of the linear prediction. Number of stimuli increased from the center toward the periphery. *E*: summation results when the number of stimuli increased from the periphery toward the center. Solid crosses centered with data points in *B*–*E* indicate cumulative SD for predicted values and SD for measured values. *F*: responses to fast (2 c/s) dot motion at -45° elevation preceded at 3 different time delays by slow (0.5 c/s) dot motion at -15° elevation (right of the vertical line). Filled triangles indicate the mean \pm SD obtained from 5 animals, top and bottom open triangles indicate responses of those 2 animals showing maximal and minimal summation, respectively (error bars indicate \pm SD from 5 repetitions). Responses to single station stimuli are shown left of the vertical line.

single station stimulation (squares and triangles, respectively, in Fig. 8, *A*, *D*, and *E*). The experimental design and data presentation are identical to those in Fig. 8*B*. In the first experiment, the number of stations activated was increased from the eye equator outward (Fig. 8*D*, insets), whereas in the second experiment, the stations were activated from the periphery inward (Fig. 8*E*, insets). In both protocols, summation was strongly sublinear and independent of the number of activated stations. Identical results were also obtained at a speed of 0.2 c/s.

Finally, we tested whether the timing of station activation might alter summation. In this experiment, the azimuth was also fixed at 90° . The first activated station had an elevation of -15° and a disc speed of 0.5 c/s. Following a variable delay, the second station was activated at an elevation of -45° and a disc speed of 2 c/s (Fig. 8*F*, insets). The difference in speeds was chosen to mimic the situation of a looming stimulus approaching along the lateral eye axis. Such stimuli elicit maximal excitation in the LGMD/DCMD and edge motion occurs first close to the equator and later toward the periphery at an increased speed. Figure 8*F* shows the outcome of this experiment: the mean firing rate averaged across five animals (filled triangles) is plotted as a function of delay and showed no

summation compared with the responses elicited by single stations alone. Similar results are shown for the two individual animals that exhibited maximal and minimal summation, respectively (Fig. 8*F*, open triangles).

Thus spatial and temporal summation of local motion stimuli is strongly sublinear at the level of the LGMD/DCMD firing rate under a wide range of experimental conditions.

DISCUSSION

This study characterized the local sensitivity and speed tuning as well as the impact of spatial and temporal interactions between local inputs within the receptive field of the LGMD/DCMD. We determined both the density of optical axes and the neuron's local sensitivity to motion. Contrary to prior expectations based on the correlation between anatomy and interneuron receptive field structure observed in other systems (e.g., Jacobs and Theunissen 2000; Krapp et al. 1998), these two distributions are largely out of register with each other. We also measured the local speed dependence of the LGMD/DCMD responses in a range from 0.2 to 4.0 c/s at many positions within the neuron's receptive field. At all locations, responses exhibit a speed dependence that can be accurately

described by a two-parameter logarithmic function. Experiments on spatial and temporal integration reveal that the LGMD combines local inputs in a strongly sublinear way. Furthermore, the latency of responses was found to depend both on speed and position within the LGMD's receptive field. Taken together, our results are in clear contrast to earlier biophysical models, which assumed the LGMD to be a linearly and uniformly summing unit (Edwards 1982; Rind and Bramwell 1996). Instead, the integration of local motion information in this neuron seems to be considerably more complex than previously thought. The LGMD is most sensitive to looming stimuli approaching on a collision course with the animal and is thus expected to play an important role in collision avoidance (Gabbiani et al. 2004; Rind and Simmons 1992; Schlotterer 1977). The characterization of the spatial input structure to the LGMD and of the local aspects of its visual responses to motion is a necessary prerequisite to understanding how its sensitivity to looming stimuli arises.

Optical measurements

The mapping of ommatidial axes based on the pseudopupil method has been successfully applied to many compound eyes in the past (e.g., Land 1997). Our work introduces one major innovation with respect to earlier studies: we used interactive programs and digital image registration techniques to facilitate the mapping of deep pseudopupils across neighboring images. This allowed us to handle the large amount of data needed to reconstruct an entire eye. Image registration was particularly useful to avoid potential reconstruction errors, because inappropriately selected markers led to large mismatches between the reference and transformed images. After correct registration, marking facets between two deep pseudopupils was reduced to a mechanical task because facet rows were aligned across images. This also considerably reduced the risk of errors. Accordingly, our reconstruction showed only few inconsistencies and allowed us to follow individual ommatidial rows over most of the eye lattice (Fig. 2, A and B). If we assume conservatively a mistake of one facet per map, the total estimated number of facets would change by 5%. This suggests our reconstruction to be a faithful indication of the density of optical axes.

The density distribution in *S. gregaria* is in good qualitative agreement with an earlier study limited to the frontal eye region of *Locusta migratoria*, in which an acute zone was also reported (Horridge 1978). The minimum interommatidial angle in *L. migratoria* was about 1.0° compared with 0.95° in *S. gregaria*. Horridge (1978) also found a similar decrease in axes density from the maximum in the frontal equatorial region. Other common features, also characteristic for other flying insects, include a region of binocular overlap in the frontal visual field and a visual streak along the eye equator (Land and Nilsson 2002).

Because of the considerable amount of work required to reconstruct a complete ommatidial lattice, this work was confined to a single female locust eye. Measurements of the local orientation of facet rows at four positions in five additional animals suggested little variability (METHODS) and thus confirmed the reliability of the results across animals. Some insect species, such as flies, exhibit a sexual dimorphism in eye structure that is most conspicuous in the degree of binocular

overlap and at the level of the acute zone (Beersma et al. 1977; Land and Eckert 1985). Typically, acute zones are located at $20\text{--}30^\circ$ higher elevations in males than females and possess a higher optical axes density ($\sim 20\text{--}30\%$). No sexual dimorphism has been reported in *L. migratoria* (Horridge 1978), and our own visual inspections of male and female eyes do not suggest such phenomenon to be present in *S. gregaria*. Intersex variations, if present at all, are therefore expected to be subtle and would only minimally affect the correlation between visual axes density and motion sensitivity reported in Fig. 6. Our results thus equally apply to both females and males.

Distribution of optical axes and motion sensitivity

The excitatory afferents project to the LGMD from the medulla through the second optic chiasm. Their anatomical organization seems to be stereotyped and retinotopic, in agreement with the general architecture of insect and crustacean visual systems (Strausfeld and Nüssel 1981). Thus the higher density of optical axes in the frontal region of the eye equator was expected to result in a higher sensitivity to motion. Rather surprisingly, exactly the opposite holds true (Fig. 4). Several factors might explain this observation. First, the weaker frontal sensitivity could very likely result from the large electrotonic distance between the corresponding synaptic inputs to the LGMD and its spike initiation zone. The orientation of the LGMD excitatory field within the lobula is such that its dendrites originate from a sturdy base corresponding to the caudo-equatorial part of the visual receptive field. The tips of the distal dendrites that sample the frontal receptive field are located $>300\ \mu\text{m}$ from the base. Thus the caudal region on the equator with the highest sensitivity to motion is also the closest to the spike initiation zone, while the frontal region is located most distant to it. Recent compartmental modeling confirmed a substantial attenuation of electrical signals along the dendritic branches of the LGMD (Peron et al. 2003). Electrotonic distance is unlikely to explain the drop in motion sensitivity with elevation, since the anatomical positions of dendritic inputs corresponding to a fixed azimuth appear to be at similar distances from the spike initiation zone. Thus a second factor that could also contribute to the motion sensitivity gradient is a systematic change of the afferent synaptic weights or of the density of synaptic contacts with elevation.

Interestingly, when the LGMD/DCMD is challenged with looming stimuli presented at different locations within its receptive field, peak firing barely decreases along the eye equator from the caudal toward the frontal visual field. Instead, it remains almost constant, within an azimuth range of $30\text{--}150^\circ$. Only toward 0 and 180° does the peak firing rate drop considerably, simply because the stimulus during the final phase of the approach exceeds the margins of the receptive field (Gabbiani et al. 2001; Rogers et al. 2003). Our findings in combination with the studies mentioned suggest a position dependent mechanism that compensates for the differences in input density during looming.

Speed tuning

We tested local speed tuning in the LGMD/DCMD over a four-octave range, $0.2\text{--}4.0\ \text{c/s}$, corresponding to equivalent retinal speeds between 6.5 and $130.4\ \text{deg/s}$ (see METHODS).

These values nearly covered the entire dynamic range of responses to local motion stimuli, from very low to near saturation at the highest speed (Fig. 5). The dependence of the LGMD/DCMD firing rate on disc speed could be described by the same functional form at all 36 measuring positions. This suggests that the processing of motion presynaptic to the LGMD follows a similar scheme across its receptive field. The increase in firing rate of the LGMD/DCMD on increasing disc speed could be due to a combination of several factors. One possibility is that presynaptic afferents to the LGMD respond with higher firing rates to faster luminance transients over the range of speeds tested. Presynaptic network effects might also contribute to an increase in excitation with disc speed. Lateral inhibition, for example, is known to exist between adjacent presynaptic afferents and is expected to be less effective as speed increases, because of the fixed transmission delay imposed by the intervening inhibitory synapse. Within the LGMD, the temporal summation of excitatory postsynaptic potentials could also contribute to an increase in firing rate with speed. However, summation was not observed in experiments where two discs were activated simultaneously or at various delays, suggesting that this effect is not preponderant. Thus the results reported here are compatible with the suggestion that the excitatory dendritic field receives local, speed-dependent input (Gabbiani et al. 1999; Hatsopoulos et al. 1995). This assumption would also explain the speed tuning observed for edges translating across the visual field (Simmons and Rind 1992). Recent extracellular recordings from nondirectionally selective units in the medulla, the neuropil immediately distal to the LGMD, exhibit a similar tuning to disc motion (Cohen and Gabbiani 2003).

Response latency and dendritic anatomy

In the present experiments, the abrupt onset of disc motion caused a reproducible early response of the LGMD/DCMD across repeated trials. Such abrupt transient responses may be important to detect sudden brief movements under natural conditions, but will not occur during smooth edge motion, as experienced during the approach of a looming object. We thus separated the transient component of the LGMD/DCMD response from the sustained one in most of our analysis. However, we took advantage of the transient response to quantify the latency between stimulus onset and the occurrence of the first DCMD spike. We analyzed only responses to stimuli which did not exceed the margins of the locust visual field; i.e., responses from 0° to 150° azimuth and from -45° to 45° elevation. The latency depended on stimulus speed with higher speeds resulting in shorter response latencies ≤ 2 c/s. Rowell et al. (1977) reported a decrease in response latency of the LGMD with an increase in light intensity or stimulus size. In addition, we also found the response latency to depend on stimulus position within a range of azimuths (Fig. 6). At low speeds, the latency decays steeply along the azimuth from 0° toward an asymptotic value reached at 60° . Because of the retinotopic arrangement of the afferent fibers to the LGMD, stimulation in the frontal visual field activates excitatory inputs to the distal branches of the excitatory field, while stimulation in the caudal visual field activates inputs close to the spike initiation zone. The latency differences therefore might be explained in part by electrotonic propagation delays. Propaga-

tion delays on the order of 10 ms along the excitatory dendritic field have been recently predicted from a passive compartmental model of the LGMD (Peron et al. 2003; centroid delays as in Zador et al. 1995).

Sublinear summation of local motion inputs

All our spatial and temporal integration experiments show that the LGMD sums local motion inputs in a strongly sublinear way. This result is surprising since the strong build-up of excitation observed in the LGMD during looming has been thought to arise from summation of local motion signals as an object grows larger on the retina (Rind and Bramwell 1996). In our experiments, the two tested speeds, 0.2 and 2.0 c/s, covered the low and middle-high end of the LGMD dynamic range for local motion stimuli, respectively. The relative activation of two local motion stimuli was varied over a time window that leads to substantial summation during looming. Furthermore, the size of the moving discs was well below that of looming stimuli or moving edges eliciting maximal firing rates ($25\text{--}35$ and $\geq 15^\circ$, respectively; Gabbiani et al. 1999; Simmons and Rind 1992). Given that no summation was observed under these conditions, we expect sublinear summation to hold over a wide range of parameters, irrespective of the relative timing, the particular speed or the size of locally activated motion stimuli. Our experiments do not, however, exclude the possibility that a simultaneous change in size and speed combined with an optimal delay will result in a different summation scheme. These results indicate that the sensitivity of the LGMD to looming is mediated by a more complex mechanism than linear summation of local excitation as an object expands across its receptive field.

Sublinear summation was independent of the number of inputs activated and of their absolute and relative location, suggesting a postsynaptic mechanism independent of dendritic location. An outward, depolarization-activated conductance similar to that responsible for dendritic gain control in non-spiking local interneurons in the locust (Laurent 1993) might explain our results. Alternatively, the feed-forward inhibitory pathways impinging on the inhibitory dendritic fields of the LGMD could be activated in parallel to the excitatory retinotopic inputs by our moving discs and prevent their summation. Feed-forward inhibition is activated by local stimuli of size similar to that used in this study (Rowell et al. 1977). It is also known to influence the responses of the LGMD during looming when the object size is still relatively small (Gabbiani et al. 2002). However, feed-forward inhibition is more effectively activated by transient stimuli, suggesting that its effect should be more pronounced at higher speeds. Our results suggest that strong sublinear summation is independent of speed for the two values tested. A weaker sublinear spatial summation has also been reported in wide-field lobula plate interneurons in the fly visual system, but it depends on the spatial separation between local stimuli (Haag et al. 1992). The underlying physiological mechanism is thought to be based on a gradual decrease of the driving force on an increase in the number of locally activated excitatory inputs (Borst et al. 1995). This model is unlikely to explain our results since we observed that sublinear summation in the LGMD is independent of stimulus separation.

In summary, the integration of local excitatory inputs sensitive to motion within the LGMD is highly nonlinear and

seems to be influenced by at least three factors: 1) the temporal and synaptic properties of presynaptic afferent fibers to the excitatory dendritic field; 2) the extended dendritic structure of the LGMD; and 3) the additional activation within the LGMD dendritic tree of either inhibitory synaptic conductances or of voltage-gated outward conductances. Because the LGMD is accessible to intracellular recordings *in vivo*, it provides a unique opportunity to investigate how these biophysical mechanisms underlie selectivity to looming and to clarify their role in the context of well-defined visually guided behaviors.

ACKNOWLEDGMENTS

The authors thank Dr. M. Burrows for lending the digital camera and Dr. H. Dahmen for assistance with the goniometer. Part of the electrophysiological measurements were performed in the laboratory of Dr. M. Egelhaaf; the authors thank him for the hospitality. Thanks to Dr. I. Cohen, S. Peron, and Dr. S. Rogers for comments on the manuscript.

GRANTS

This work was supported by funds of the National Institute of Health, an Alfred P. Sloan Fellowship to F. Gabbiani, and the Royal Society to H. G. Krapp.

REFERENCES

- Ball W and Tronick E.** Infant responses to impending collision: optical and real. *Science* 171: 818–820, 1971.
- Beersma DGM, Stavenga DG, and Kuiper JW.** Organization of the visual axes in the compound eye of the fly *Musca domestica* L. and behavioural consequences. *J Comp Physiol* 102: 305–320, 1975.
- Beersma DGM, Stavenga DG, and Kuiper JW.** Retinal lattice, visual field and binocularities in flies. Dependence on species and sex. *J Comp Physiol* 119: 207–220, 1977.
- Borst A, Egelhaaf M, and Haag J.** Mechanisms of dendritic integration underlying gain control in fly motion sensitive interneurons. *J Comput Neurosci* 2: 5–18, 1995.
- Burrows M and Rowell CHF.** Connections between descending visual interneurons and metathoracic motoneurons in the locust. *J Comp Physiol* 85: 221–234, 1973.
- Cohen I and Gabbiani F.** Multielectrode extracellular recordings from the locust optic lobe. *Program No. 491.4 Abstract Viewer/Itinerary Planner*. Washington, DC: Society of Neuroscience, 2003.
- Dahmen H.** Eye specialisations in water striders: an adaptation to life in a flat world. *J Comp Physiol A* 169: 623–632, 1991.
- Edwards DH.** The cockroach DCMD neurone I. Lateral inhibition and the effect of light- and dark-adaptation. *J Exp Biol* 99: 61–90, 1982.
- Franceschini N and Kirschfeld K.** Les phénomènes de pseudopupille dans l'oeil composé de *Drosophila*. *Kybernetik* 9: 159–182, 1971.
- Gabbiani F, Krapp HG, Hatsopoulos N, Mo CH, Koch C, and Laurent G.** Multiplication and stimulus invariance in a looming-sensitive neuron. *J Physiol Paris* 98: 19–34, 2004.
- Gabbiani F, Krapp HG, Koch C, and Laurent G.** Multiplicative computation in a visual neuron sensitive to looming. *Nature* 420: 320–324, 2002.
- Gabbiani F, Krapp HG, and Laurent G.** Computation of object approach by a wide-field motion-sensitive neuron. *J Neurosci* 19: 1122–1141, 1999.
- Gabbiani F, Mo CH, and Laurent G.** Invariance of angular threshold computation in a wide-field looming-sensitive neuron. *J Neurosci* 21: 3144–329, 2001.
- Gibson JJ.** *The Ecological Approach to Visual Perception*. Boston, MA: Houghton Mifflin, 1979.
- Gray JR, Lee JK, and Robertson RM.** Activity of descending contralateral movement detector neurons and collision avoidance behavior in response to head visual stimuli in locusts. *J Comp Physiol A* 187: 115–129, 2001.
- Haag J, Egelhaaf M, and Borst A.** Dendritic integration of motion information in visual interneurons of the blowfly. *Neurosci Lett* 140: 173–176, 1992.
- Hatsopoulos N, Gabbiani F, and Laurent G.** Elementary computation of object approach by a wide-field visual neuron. *Science* 270: 1000–1003, 1995.
- Horridge GA.** The separation of visual axes in apposition compound eyes. *Philos Trans R Soc Lond B Biol Sci* 285: 1–59, 1978.
- Jacobs GA and Theunissen FE.** Extraction of sensory parameters from a neural map by primary sensory interneurons. *J Neurosci* 20: 2934–2943, 2000.
- Judge S and Rind FC.** The locust DCMD neuron, a movement-detecting neurone tightly tuned to collision trajectories. *J Exp Biol* 200: 2209–2216, 1997.
- Killmann F, Gras H, and Schürmann F-W.** Types, numbers and distribution of synapses on the dendritic tree of an identified visual interneuron in the brain of the locust. *Cell Tissue Res* 296: 645–665, 1999.
- Klette R and Zamperoni P.** *Handbook of Image Processing Operators*. Chichester, UK: John Wiley, 1996.
- Krapp HG and Hengstenberg R.** A fast stimulus procedure for determining local receptive-field properties of motion-sensitive visual interneurons. *Vision Res* 37: 225–234, 1997.
- Krapp HG, Hengstenberg B, and Hengstenberg R.** Dendritic structure and receptive-field organization of optic flow processing interneurons in the fly. *J Neurophysiol* 79: 1902–1917, 1998.
- Land MF.** Visual acuity in insects. *Annu Rev Entomol* 42: 147–177, 1997.
- Land MF and Eckert H.** Maps of acute zones of fly eyes. *J Comp Physiol A* 156: 525–538, 1985.
- Land MF and Nilsson DE.** *Animal Eyes*. Oxford, UK: Oxford, 2002.
- Laurent G.** A dendritic gain control mechanism in axonless neurons of the locust, *Schistocerca americana*. *J Physiol* 470: 45–54, 1993.
- Luksch H, Khanbabaie R, and Wessel R.** Synaptic dynamics mediate sensitivity to motion independent of stimulus details. *Nat Neurosci* 7: 380–388, 2004.
- Matheson T, Krapp HG, and Rogers SM.** Plasticity in the visual system is correlated with a change in lifestyle of solitary and gregarious locusts. *J Neurophysiol* 91: 1–12, 2004.
- O'Shea M and Rowell CHF.** Protection from habituation by lateral inhibition. *Nature* 254: 53–55, 1975.
- O'Shea M and Rowell CHF.** The neuronal basis of a sensory analyser, the acridid movement detector system. II. Response decrement, convergence, and the nature of the excitatory afferents to the fan-like dendrites of the LGMD. *J Exp Biol* 65: 289–308, 1976.
- O'Shea M and Williams JLD.** Anatomy and output connections of the lobular giant movement detector neuron (LGMD) of the locust. *J Comp Physiol* 91: 257–266, 1974.
- Pauluis Q and Baker SN.** An accurate measure of the instantaneous firing discharge probability, with application to unitary joint-event analysis. *Neur Comput* 12: 647–669, 2000.
- Pearson KG, Heitler WJ, and Steeves JD.** Triggering of locust jump by multimodal inhibitory interneurons. *J Neurophysiol* 43: 257–278, 1980.
- Peron SP, Krapp HG, Laurent G, and Gabbiani F.** Role of dendritic morphology in the processing of looming stimuli: a compartmental modeling study. *Program No. 491.3. Abstract Viewer/Itinerary Planner*. Washington, DC: Society of Neuroscience, 2003.
- Petrowitz R, Dahmen H, Egelhaaf M, and Krapp HG.** Arrangement of optical axes and spatial resolution in the compound eye of the female blowfly *Calliphora*. *J Comp Physiol A* 186: 737–746, 2000.
- Press WH, Teukolsky SA, Vetterling WT, and Flannery BP.** *Numerical recipes in C*, 2nd ed. Cambridge: Cambridge University Press, 1992.
- Richmond BJ, Optican LM, and Spitzer H.** Temporal encoding of two-dimensional patterns by single units in primate visual cortex. I. Stimulus-response relations. *J Neurophysiol* 64: 351–369, 1990.
- Rind FC and Bramwell DI.** Neural network based on the input organization of an identified neuron signalling impending collision. *J Neurophysiol* 75: 967–985, 1996.
- Rind FC and Santer RD.** Collision avoidance and a looming sensitive neuron: size matters but biggest is not necessarily best. *Proc R Soc Lond B Suppl* 3: S27–S29, 2003.
- Rind FC and Simmons PJ.** Orthopteran DCMD neuron: a reevaluation of responses to moving objects. I. Selective responses to approaching objects. *J Neurophysiol* 68: 1654–1666, 1992.
- Robertson RM and Johnson AG.** Retinal image size triggers obstacle avoidance in flying locusts. *Naturwiss* 80: 176–178, 1993.
- Rogers SM, Harston GWJ, Kilburn-Toppin F, Matheson T, and Krapp HG.** Receptive field organization of a collision-detecting visual interneuron in solitary and gregarious locusts. *J Physiol* 555P: PC130, 2003.
- Rowell CHF.** The orthopteran descending movement detector (DMD) neurones: a characterization and review. *Z Vergl Physiol* 73: 167–194, 1971.
- Rowell CHF, O'Shea M, and Williams JLD.** The neuronal basis of a sensory analyser, the acridid movement detector system. IV. The preference for small field stimuli. *J Exp Biol* 68: 157–185, 1977.

- Schiff W.** Perception of impending collision: a study of visually directed avoidant behavior. *Psychol Monogr* 79: 1–26, 1965.
- Schlotterer GR.** Response of the locust descending movement detector neuron to rapidly approaching and withdrawing visual stimuli. *Can J Zool* 55: 727–747, 1977.
- Sherk H and Fowler GA.** Neural analysis of visual information during locomotion. *Prog Brain Res* 134: 247–264, 2001.
- Simmons PJ and Rind FC.** Orthopteran DCMD neuron: a reevaluation of responses to moving objects. II. Critical cues for detecting approaching objects. *J Neurophysiol* 68: 1667–1682, 1992.
- Strausfeld NJ and Nüssel DR.** Neuroarchitectures serving compound eyes of crustacea and insects. In: *Handbook of Sensory Physiology*, vol. VII/7B, edited by Autrum H. Berlin: Springer, 1981, p. 1–132.
- Stavenga DG.** Pseudopupils of compound eyes. In: *Handbook of Sensory Physiology*, vol. VII/6A, edited by Autrum H. Berlin: Springer, 1979, p. 357–439.
- Sun H and Frost BJ.** Computation of different optical variables of looming objects in pigeon nucleus rotundus neurons. *Nat Neurosci* 1: 296–303, 1998.
- Wicklein M and Strausfeld NJ.** Organization and significance of neurons that detect change of visual depth in the hawk moth *Manduca sexta*. *J Comp Neurol* 424: 356–376, 2000.
- Yamamoto K, Nakata M, and Nakagawa H.** Input output characteristics of collision avoidance behaviour in the frog *Rana catesbeiana*. *Brain Behav Evol* 62: 201–211, 2003.
- Zador AM, Agmon-Snir H, and Segev I.** The morphoelectronic transform: a graphical approach to dendritic function. *J Neurosci* 15: 1669–1682, 1995.